sustainability

MDPI

Article

The Direct Reduction of Iron Ore with Hydrogen

Shuo Li [1], Huili Zhang [2], Jiapei Nie [2], Raf Dewil [3], Jan Baeyens [1,3] and Yimin Deng [3,*]

[1] Beijing Advanced Innovation Centre for Smart Matter Science and Engineering, Beijing University of Chemical Technology (BUCT), Beijing 100029, China; ssurel@mail.buct.edu.cn (S.L.); baeyens.j@gmail.com (J.B.)
[2] School of Life Science and Technology, Beijing University of Chemical Technology (BUCT), Beijing 100029, China; zhhl@mail.buct.edu.cn (H.Z.); niejiapei@163.com (J.N.)
[3] Process and Environmental Technology Lab, Department of Chemical Engineering, KU Leuven, J. De Nayerlaan 5, 2860 Sint-Katelijne-Waver, Belgium; raf.dewil@kuleuven.be
* Correspondence: yimin.deng@kuleuven.be

Abstract: The steel industry represents about 7% of the world's anthropogenic CO_2 emissions due to the high use of fossil fuels. The CO_2-lean direct reduction of iron ore with hydrogen is considered to offer a high potential to reduce CO_2 emissions, and this direct reduction of Fe_2O_3 powder is investigated in this research. The H_2 reduction reaction kinetics and fluidization characteristics of fine and cohesive Fe_2O_3 particles were examined in a vibrated fluidized bed reactor. A smooth bubbling fluidization was achieved. An increase in external force due to vibration slightly increased the pressure drop. The minimum fluidization velocity was nearly independent of the operating temperature. The yield of the direct H_2-driven reduction was examined and found to exceed 90%, with a maximum of 98% under the vibration of ~47 Hz with an amplitude of 0.6 mm, and operating temperatures close to 500 °C. Towards the future of direct steel ore reduction, cheap and "green" hydrogen sources need to be developed. H_2 can be formed through various techniques with the catalytic decomposition of NH_3 (and CH_4), methanol and ethanol offering an important potential towards production cost, yield and environmental CO_2 emission reductions.

Keywords: hydrogen; iron ore; direct reduction; fluidized bed; solar energy

check for updates

Citation: Li, S.; Zhang, H.; Nie, J.; Dewil, R.; Baeyens, J.; Deng, Y. The Direct Reduction of Iron Ore with Hydrogen. *Sustainability* **2021**, *13*, 8866. https://doi.org/10.3390/su13168866

Academic Editor: Miguel Ángel Reyes Belmonte

Received: 30 June 2021
Accepted: 5 August 2021
Published: 8 August 2021

Publisher's Note: MDPI stays neutral with regard to jurisdictional claims in published maps and institutional affiliations.

Copyright: © 2021 by the authors. Licensee MDPI, Basel, Switzerland. This article is an open access article distributed under the terms and conditions of the Creative Commons Attribution (CC BY) license (https://creativecommons.org/licenses/by/4.0/).

1. Introduction

1.1. Background Information

Most steel mills are currently using the blast furnace principle, fuelled by mostly coal, coke and coke oven gas. The successive processes of sinter belt, blast furnace and converter operate at extremely high temperatures, hence being energy-intensive and producing significant amounts of CO_2. The steel industry represents about 7% of the world's anthropogenic CO_2 emissions. Within the objectives of COP21 (Paris, 2015), the target of steel mills is to reduce the CO_2 emissions from the current (nearly) 3000 Mton/year to below 500 Mton/year. The use of renewable energy sources is, hence, a topic of major development, and ultimately the CO_2-lean direct reduction of iron ore with hydrogen is considered to offer high potential. Two alternative direct H_2 ore reductions (Figure 1, right-side) and the traditional fossil-fuel blast furnace operation (Figure 1, left-side) are illustrated in Figure 1 below.

Whereas the production of sponge iron from iron ore pellets is already commercially applied, the direct H_2 reduction of crude iron ore powder has the advantages of omitting the sintering stage that is the major energy consumer and CO_2 emission source of the iron-making process, together with the blast furnace. Sintering is indeed required to produce a sinter cake to be loaded into the blast furnace. It thermally agglomerates the mixture of iron ore fines, recycled iron-making products, fluxes, slag-forming agents and solid fuel (coke) at a temperature between 1300 and 1480 °C. Omitting the sintering operation will hence reduce the overall energy consumption and CO_2 emissions by 35 to 40% [1].

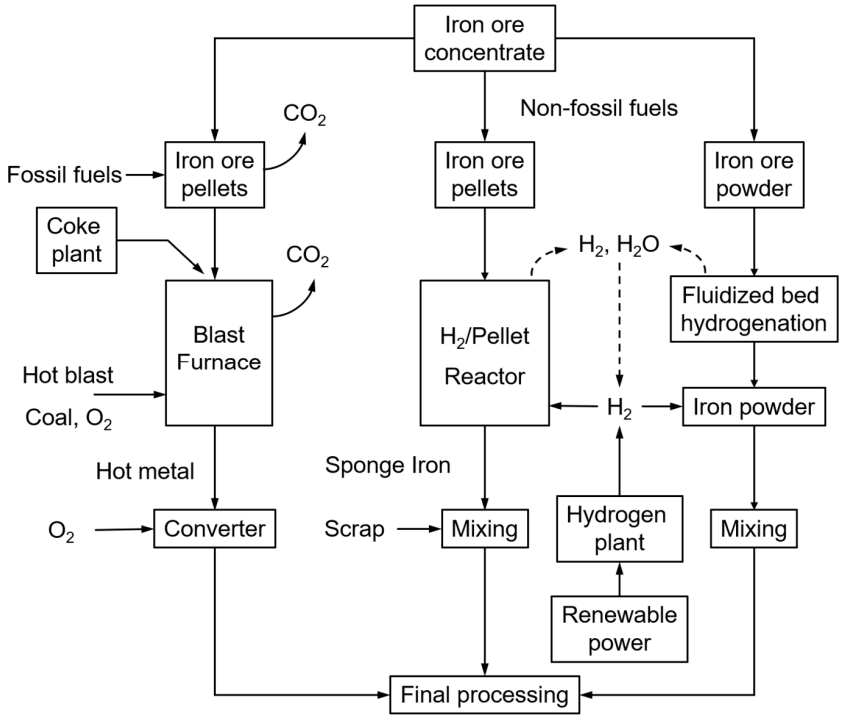

Figure 1. Different steel-making processes: traditional, using fossil fuels (**left**); H_2-driven (**right**).

The main reasons behind researching the reduction of CO_2 using hydrogen are based upon limiting both the required thermal energy and the associated CO_2 emissions.

Major developments were reported since 2015, with research efforts illustrated in Figure 2. This figure was established from Web of Science statistics with appropriate keywords. Over 70% of the research dealt with the fundamentals of direct ore reduction using hydrogen and the reactors to be used (rotary furnace, plasma, fixed and fluidized beds). Additional publications tentatively focused upon process economics and environmental benefits. The fixed/moving or fluidized bed reactors represent only 7 out of 28 papers (see Table 1), stressing the need for additional research, as dealt with in the present study.

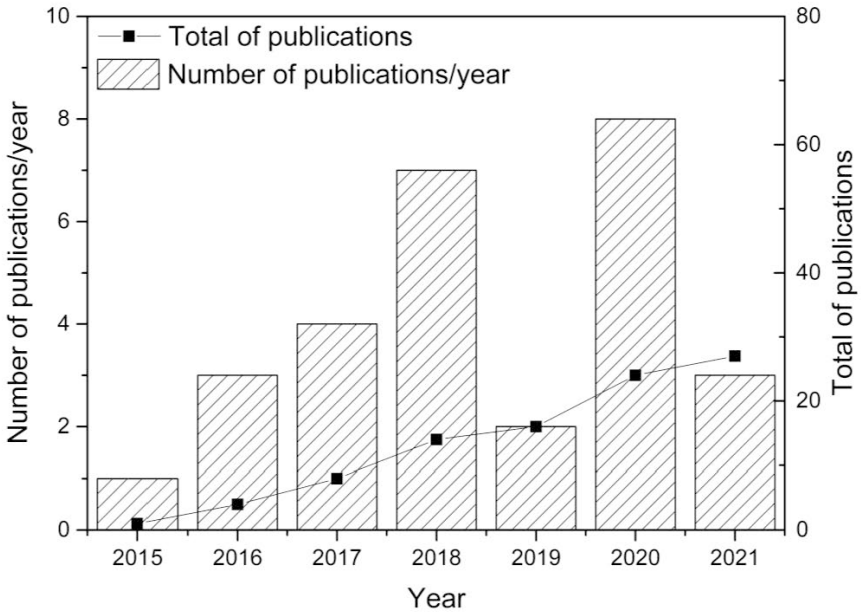

Figure 2. Review of publications since 2015, from Web of Science, with keywords iron ore, direct reduction, hydrogen, CO_2 reduction.

Table 1. Important research contributions since 2017.

References	Major Findings
	Hydrogen reduction of iron ores
Sohn et al. [2]	Developed a novel iron-making technology based on fine iron ore concentrate in a flash reactor. Optimization towards using multiple burners, preheating the feed gas, or both is examined.
Abolpour et al. [3]	Studied the reaction kinetics of H_2 reduction of iron ore concentrate particles between 700 and 900 °C.
Murakami et al. [4]	Studied the effect of H_2 concentration in the reducing gas on the changes in mineral phases during reduction of iron ore sinter. The mineral composition of 10 types of sinter samples was analyzed.
Patisson & Mirgauxb [5]	Analyzed a new route for making steel from iron ore based on the use of H_2, with a 90% reduction in CO_2 emissions compared to those of the blast-furnace route.
Zhang et al. [6]	Described the reduction kinetics by a pellet-scale single-interface shrinking core model at temperatures below 1143 K. At higher temperatures, the rate-limiting step is the interfacial chemical reaction process.
Bai et al. [7]	Investigated the thermal reduction of pellets by H_2. An un-reacted core and interfacial chemical reaction are reaction rate controlling steps in function of the operating temperature.
Wei et al. [8]	Conducted reduction experiments with a H_2-N_2 mixture in a rotary drum reactor. A dense, increasingly thick layer of iron was formed during the reduction reaction. The reduction process was controlled by a first-order reaction model.
Bai et al. [9]	Studied the direct reduction behavior and dynamic characteristics of oxidized pellets under the 75% H_2-25% N_2 atmosphere at 760, 900, 1000 °C. Holes and cracks were observed at higher temperature, hampering the reduction degradation behavior of the pellets.
Lyu et al. [10]	Investigated the effect of hydrogen addition on gas utilization in a blast furnace. The H_2 content should be controlled in the range of 5%–10%.
Elzohiery et al. [11]	Demonstrated that the reduction is of a first-order dependence with the hydrogen partial pressure.
Du et al. [12]	Proposed a new process that could simultaneously enrich CH_4 from coke oven gas and produce separated magnetite from low-grade hematite.
Sohn et al. [13]	Reduced the concentrate by H_2 and CO gas mixtures formed from the partial oxidation of natural gas in a flash reactor. The rate equations were applied to experimental results from a laboratory flash reactor using CFD simulation.
Htet et al. [14]	Investigated the gasification reactivity of carbon black compared to the carbonaceous materials used in the HIsarna process by TGA method at 1250 °C, 1350 °C and 1450 °C under atmospheric pressure. Carbon black is less reactive than thermal coal and charcoal. The random pore model best describes the gasification reaction of the selected samples. Activation energies were determined.
	Energetic and environmental importance of H_2-based steel production
Bhaskar et al. [15]	Developed a mass and energy flow model based upon Python to explore the feasibility of using H_2- direct reduction of iron ore (HDRI) coupled with an electric arc furnace (EAF) for carbon-free steel production. This technology could reduce specific emissions from steel production in the EU by more than 35%, at present grid emission levels (295 $kgCO_2$/MWh).
Vogl et al. [16]	Hydrogen direct reduction (H-DR) steelmaking needs 3.48 MWh of electricity per ton of liquid steel, mainly for the electrolytic hydrogen production. H-DR emits only 2.8% of blast furnace CO_2.
	Mixed/moving and fluidized bed direct reduction reactors
He et al. [17]	Investigated the micro-fluidized bed reduction behavior of Brazilian hematite in 20% H_2 and 80% Ar at 400–570 °C. The reaction rate was suggested to be determined by the phase boundary reaction.
Spreitzer & Schenk [18]	Investigated the fluidization behavior and reducibility of various iron ore grades. A stable fluidization of hematite- and limonite-based iron ores was observed, while magnetite-based iron ore could not be fluidized.
Knop and Kubiak [19]	Studies the comparison of a combined H2-based direct reduction and electric steelmaking, and the ore-fines reduction in a novel fluidized bed process.
Hamadeh et al. [20]	Studied the moving bed principle in de direct reduction shaft furnace, providing evidence of 8 different zones according to the predominant thermal and reaction characteristics.
da Costa et al. [21]	In a counter-current direct-reduction moving bed reactor, CO_2 emissions were reduced by more than 80%.
Lazou et al. [22]	Studied the CO_2 reduction in the conventional Pedersen Process by reducing iron or bauxite ore at temperatures below and above 560 °C. At temperatures above 860 °C, the formation of $FeAl_2O_4$ retards the reduction to metallic iron.
Moldenauer et al. [23]	A circulating fluidized bed reactor was applied in a chemical looping combustion. CO_2 reductions of 75 to 92% were achieved.

Some selected and important publications are listed in Table 1 according to their main output. Research on fixed/moving or fluidized ore reduction was separately included in the Table. The solar energy potential was not previously reported upon.

Similar research efforts on reducing the CO_2 emissions from thermal processes were also presented for different fields, with a specific target of CO_2 modeling, such as in a large-scale coal-fired thermal power plant [24], in integrated processing of liquified natural gas [25], in a multigeneration cascade system [26], in the pyrolysis reaction of lignocellulosic waste [27], or through the integration of rigid porous high-temperature filters in thermal processes [28], among others.

1.2. Objectives, Structure and Contribution of the Reported Research

From the literature survey, it is clear that the direct H_2-driven reduction of iron ore, and the considerably lower CO_2 emissions, are increasingly important. The previous research developed some fundamental principles about the reaction mechanisms, reduction kinetics and CO_2 reduction potential, as also dealt with in several studies about CO_2 modeling. The importance of using a zero CO_2 emission H_2 as a fuel toward CO_2 abatement in comparison with common fossil fuels is illustrated in Figure 3.

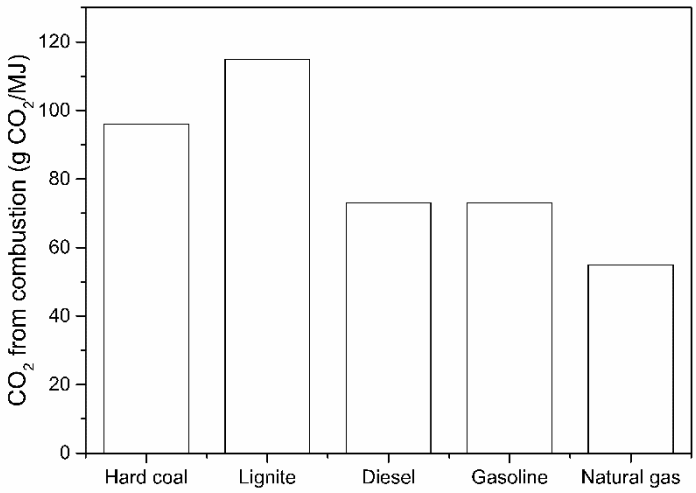

Figure 3. CO_2 emissions when burning an equivalent energy unit of fuel.

The application of fluidized bed reactors in this direct reduction principle of iron ores was only scarcely investigated. The application of sustainable solar energy was not investigated. To complete and assess the previous findings, and develop the perspective of concentrated solar energy application in the fluidized bed to direct H_2 reductions of iron ore, this paper has multiple objectives.

Firstly, the properties of the iron ore powder that can be used in a fluidized bed H_2-reduction reactor will be summarized.

Secondly, reaction fundamentals will be studied in both an isothermally operated macro-thermogravimetric reactor with electrical heating and in a vibrated fluidized bed reactor positioned in the cavity and focused on a concentrated solar furnace. Both the reduction yield and the fluidization reactor operation characteristics (velocities, pressure drop, temperature profiles within the reactor) will be determined. The results will confirm the potential of the direct H_2 reduction of iron ore in a solar fluidized bed reactor.

Thirdly, the production of "renewable" H_2 will be assessed. Although tests were performed on a lab-scale batch basis only, the economy of producing renewable H_2 will be demonstrated.

Finally, all experimental findings and future developments will be summarized in the conclusions.

These objectives are summarized in the research framework of the paper, as presented in Figure 4.

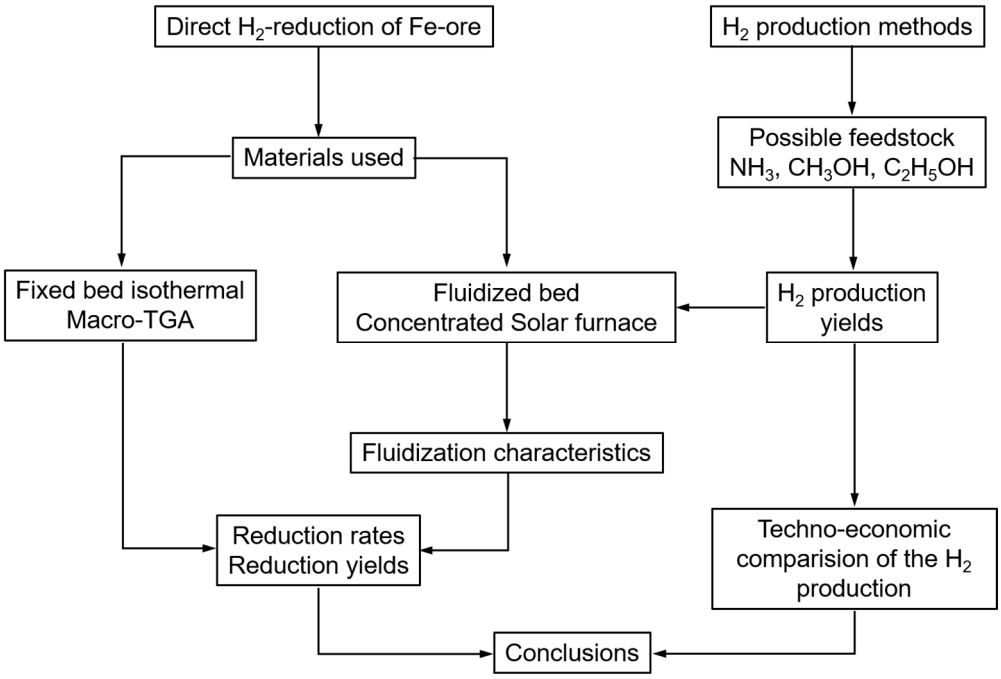

Figure 4. Research framework.

2. Materials and Methods

2.1. Materials

The physical and chemical properties of the fine Fe_2O_3 particles used to examine the fluidization and hydrogen reduction are listed in Table 2. These particles belong to the Geldart group C (cohesive) particles, based on particle size, particle density and gas density [29].

Table 2. Physical and chemical properties of fine Fe_2O_3 particles.

Particle Property	Value
Mean particle size (μm)	10–15
Particle density (kg/m^3)	4800
Shape	Non-spherical, sphericity ~0.85
Chemical composition	Iron 68%, Oxygen 30%

2.2. Methods and Procedures

2.2.1. Experimental Set-Ups

Two experimental rigs were used in the study: an electrically heated furnace and a solar-heated reactor.

Isothermal conversions under the H_2 feed were determined by a macro-thermogravimetric analyzer (electrically-heated macro-TGA), where the weight loss under the H_2 feed was monitored, according to the method described by Fernandez et al. [30]. The set-up is illustrated in Figure 5. The total heating capacity is 8 kW, and the heating rate is controlled by the thermocouple installed in the Fe_2O_3 ore bed.

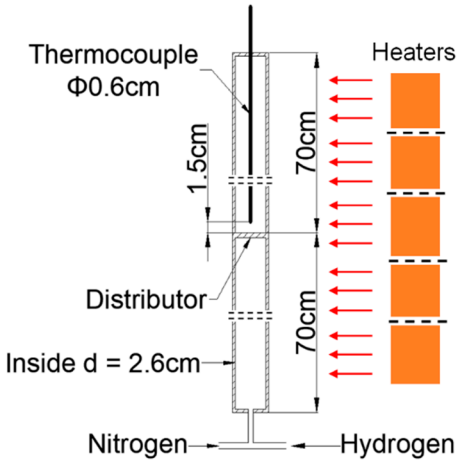

Figure 5. Lab-scale set-up (electrical furnace).

The iron ore (170 g) was loaded inside the reactor above the distributor. The static bed height was about 16 cm. The bottom section of the electrically heated reactor served as the preheating section of the gas feed. Nitrogen was used when starting the experiment. When the reactant bed temperature reached the set point of 773 K, the N_2 feed was stopped, and H_2 was fed to the reactor. The time of reaction was used as a process parameter. When the required time was reached, the feed of H_2 was stopped, N_2 was restarted, the electric heating was stopped, and the reactor was allowed to cool. Samples of feedstock and reaction products were also analyzed for their oxygen concentration.

Solar H_2 reductions were carried out in the solar thermal furnace, depicted in Figure 6. The maximum heat load in the cavity was ~20 kW. The vibrating fluidized bed was installed inside the 0.5 m × 0.5 m × 0.5 m cavity with an irradiation opening of 0.3 m diameter. Since we had to treat cohesive particles, a vibrating fluidized bed was used. The solar irradiation was collected by a heliostat and focused onto the cavity opening by a parabolic concentrator. The heat load could be controlled by partly defocusing the heliostat. A photograph of the experimental rig in operating conditions is shown in Figure 7.

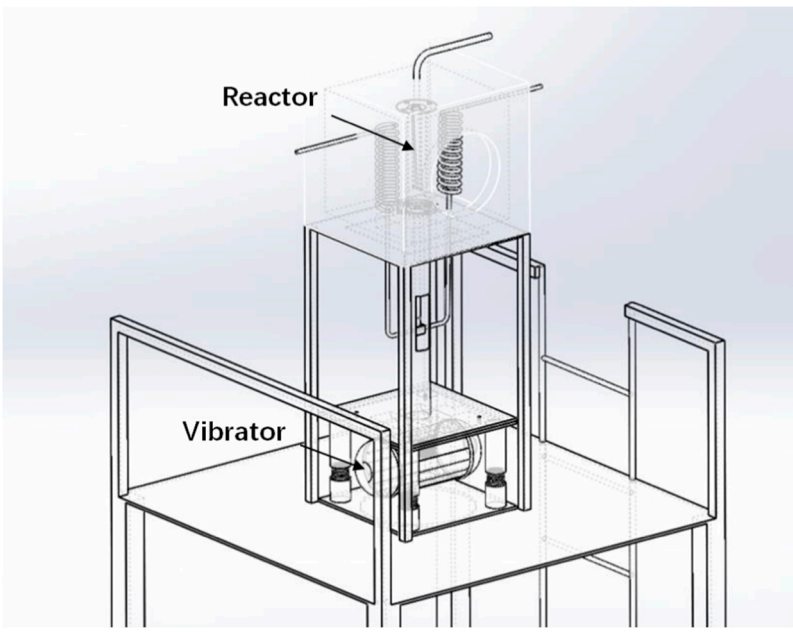

Figure 6. Schematic of the solar receiver test unit (reactor installed in the cavity).

Figure 7. Solar furnace in QinHuangDao (Hebei Province, China).

Table 3 lists the specifications of the solar test unit and test conditions. The internal diameter of the fluidized bed reactor was 50 mm. H_2 was preheated by a coil heat exchanger also installed in the cavity and visible at the right of Figure 6. About 500 g of fine Fe_2O_3 particles formed the bed. A multi-orifice distributor was used to ensure a uniform gas distribution in the fluidized bed reactor [31].

Table 3. Experimental conditions.

Parameter	
Fluidizing carrier gas	N_2
Reduction gas	H_2
Superficial gas velocity (m/s)	<0.02
Bed height (m)	0.25
Vibration frequency [Hz]	<50
Vibration amplitude [mm]	0.6
Vibration direction	Vertical
Reaction temperature [K]	773–873

The vibration of the fluidized bed reactor was applied by adjusting the motor inverter frequency. The vibration frequency could be adjusted up to 47.7 Hz, and the amplitude was fixed to 0.6 mm. The pressure drop was checked in real-time using a differential pressure transmitter (Rosemount Inc., Shakopee, MN, USA) through pressure drop ports just above the distributor and at the top of the reactor. Hydrogen was used as the reduction gas, whereas nitrogen was used as fluidization gas at start-up (till the desired bed temperature was obtained) and at shut-down. Nitrogen and hydrogen gas was supplied to the fluidized bed using separate mass flow controllers. After the reduction was performed for a given reaction time, nitrogen was injected again to reduce the temperature of the reactor to ambient temperature, and the products were collected for analysis.

2.2.2. Data Treatment

For both experimental set-ups, the representative reduction reaction rate is shown in Equation (1) and evaluated on the basis of the weight loss during the reduction process and confirmed by the O-content of the Fe_2O_3, sampled at distinct times [32,33].

$$\text{Reduction yield} = \frac{\text{Oxygen content in } Fe_2O_3 - \text{oxygen content in product}}{\text{Oxygen content in } Fe_2O_3}, \quad (1)$$

3. Results and Discussion

3.1. The Fluidization Characteristics of the Fine Fe_2O_3 Particles

Due to the cohesiveness of the particles, fluidization with gas alone was impossible. Channels and rat holes formed in the cohesive particles. To increase the fluidity of the fine particles, fluidization must be performed with the help of an external force to decrease the interparticle Van der Waals force. The vibration causes the particles to remain non-agglomerated.

Vibrated fluidization provides a uniform distribution of the gas flow, prevents the formation of particle agglomerates, and weakens the interparticle force. When the combined forces of the vibration and the hydrodynamic shear force exerted on the particles by the gas flow (related in a fluidized bed to the bed weight) exceed the Van der Waals force, fluidization of the C-type particles is achieved. The vibration force depends upon the vibration frequency and amplitude. Equation (2) defines the effective acceleration, resulting from the effects of vibration frequency and amplitude [34,35]:

$$g_{ef} = g\left(1 + \frac{A_v f^2}{g}\right), \tag{2}$$

with:
g: gravitational acceleration (9.81 m/s^2)
A_v: amplitude of the vibration (m)
f: frequency of the vibration (Hz; m/s)
g_{ef}: effective acceleration factor (m/s^2)

Without vibration, the fluidization characteristics showed excessive channeling. A bubbling fluidized regime was achieved when vibration was applied. Figure 8 shows pressure drop values for the 0.25 m deep bed of fine Fe_2O_3 particles as a function of the temperature. At reaction temperatures from 273 to 993 K, the pressure drop values at 25 Hz were 4.8 kPa, irrespective of the applied temperature. When the vibration frequency was increased, the pressure drop slightly increased by a maximum of 5%. The minimum fluidization velocity, U_{mf}, hardly changed when the frequency and/or temperature increased, although a minimum vibration frequency of ~10 Hz was required (at the constant amplitude of 0.6 mm). The minimum fluidization velocity is around 1 mm/s.

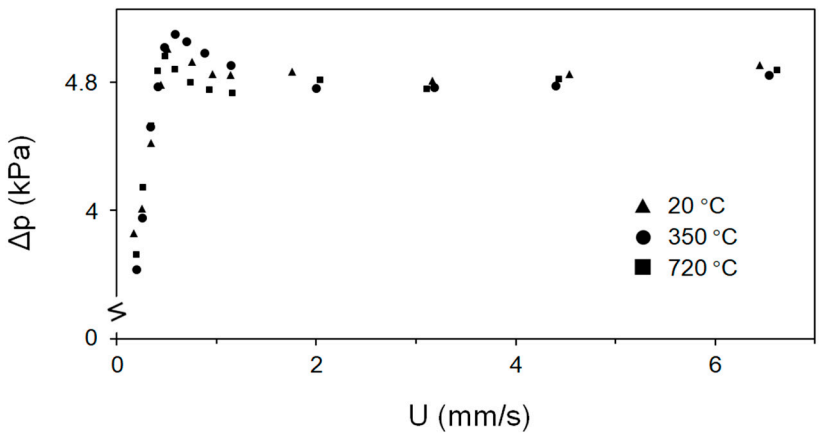

Figure 8. Pressure drop across the bed versus superficial gas velocity.

Contrary to other Geldart particle types (A, B or D particles), fluidization has no distinct temperature-dependent tendency when vibration is applied to Geldart group C particles. At a vibration frequency of 10 Hz, the U_{mf} value could not be determined because the pressure drop values for fine Fe_2O_3 particles did not exhibit a clear trend. As the external force increased, fluidization changed to the bubbling regime, with a constant pressure drop achieved in the bubbling regime.

3.2. The Fe_2O_3 Reduction Rate

Figure 9 shows the reduction yield for the vibrated fluidized bed operation. Under the specific conditions of the test, the reaction time was about 50 min for a maximum reduction yield of about 90%. Increasing the vibration frequency to 47 Hz improved the reaction, and yields close to 98% were achieved. The superficial H_2 velocity was 0.01 m/s.

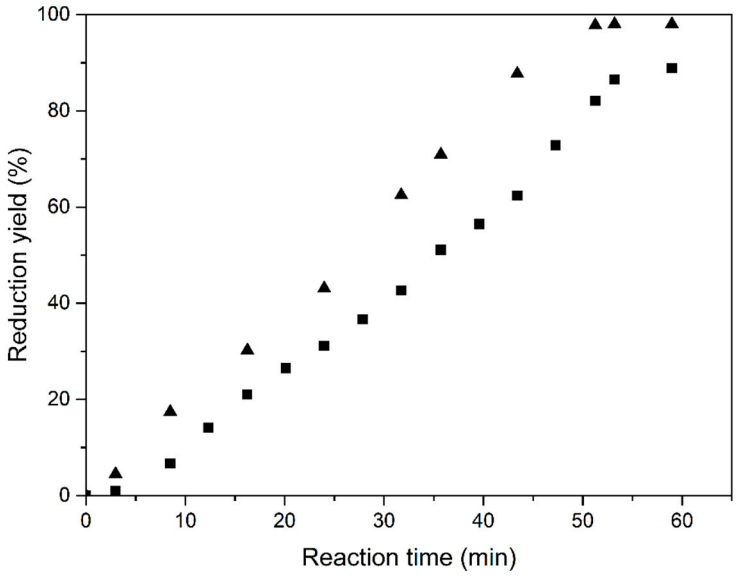

Figure 9. Reduction of Fe_2O_3 at 773 K with vibration at 20 (■) and 47 Hz (▲), respectively.

Such high Fe_2O_3 reduction rates, achieved at the low temperature of 500 °C, demonstrate that fine iron ore particles can directly be converted into Fe without prior sintering by replacing the blast furnace with a vibro-fluidized bed and direct H_2 reduction. Moreover, the application of solar heat totally eliminates the use of fossil fuels, although the fossil fuel-fired operation is also possible and can be operated at a low temperature. The potential energy savings of the direct reduction processes are considerable since neither sintering nor high-temperature blast furnace reduction is required. Since these latter processes require significant applications of fossil fuels, the CO_2 savings are evident.

The remaining important issue is the production of H_2, preferably by a "green" production method, as discussed below. The current H_2 production methods rely mostly on steam reforming of CH_4, on the gasification of coal or biomass, and on the electrolysis of water to a minor extent. Producing H_2 by non-fossil fuel resources and by avoiding gasification should therefore be of primary importance.

4. Potential "Green" H_2 Production Methods

4.1. NH_3 Decomposition

Liquid NH_3 can be considered an H_2 storage medium and can be decomposed to N_2 and H_2. Although this decomposition is currently being tested, the literature provides sufficient background data to assess the reaction feasibility.

Electrolysis and thermo-chemical processes can be utilized for NH_3 decomposition. The thermo-chemical decomposition of NH_3 involves a catalyst inside a reactor using a reaction as follows:

$$NH_3 \rightleftharpoons 0.5\,N_2 + 1.5H_2 \quad \Delta H^o = 46.2\ \mathrm{kJ/mol}$$

The decomposition reaction is an endothermic thermochemical reaction that requires high temperatures, around 250–700 °C, and relatively high NH_3 partial pressures [36].

Theoretically, the thermodynamic equilibrium calculation produces the single-pass conversion rate at different decomposition temperatures, as presented in Table 4. The

decomposition can reach a complete reaction with a conversion rate of 99% at a temperature of at least 400 °C. Higher temperatures above 450 °C no longer strongly influence the reaction but rather its kinetics [36].

Table 4. Equilibrium NH_3 decomposition (at 1 bar) as a function of temperature, with original data from [36].

Temperature (°C)	NH_3 Conversion (%)
300	95.7
400	99.1
500	99.7
600	99.9

Recent studies reported various single metal catalyst, in terms of activity, in the decreasing order Ru > Ni > Rh > Co > Ir >Fe > Pt > Cr > Pd > Cu >> Te, Se, Pb [37]. However, even if Ru shows the best conversion activity, this type of catalyst is still not sufficiently active for NH_3 decomposition at a temperature of 450 °C. More importantly, it will not be economically viable for large-scale applications. Multiple sources state that the Ru-based catalyst is active at a temperature of decomposition over 600 °C with a conversion rate of 97%.

Research and development of catalysts are done on precious metals, bimetallic materials, and metal oxides [38–42]. The bimetallic compound is proven to improve catalytic performance even though the manufacturing is complicated. It was also shown that metal oxides work by changing the electronic density of the active catalyst sites, and hence, are proposed as promoters and supporting materials for catalysts.

4.2. C_2H_5OH and CH_3OH Catalytic Decomposition

The catalytic decomposition of ethanol was studied in both the electric and solar furnaces in Figures 5–7. Results are shown in Figure 10 below for an ethanol/water mixture (1 to 6 mol-ratio), at a feed rate of 0.1 mL/min of ethanol/water and using two different catalysts, i.e., $MnFe_2O_4$ and a Co-loaded Al_2O_3.

The produced gas stream was continuously monitored by a gas chromatograph. The lag time of about 25 min is due to the piping between the reactor outlet and the GC. H_2, CO, CO_2 and CH_4 were the main products identified; acetone was also detected. The reaction mechanisms are currently under investigation.

A similar procedure was applied for the steam-methanol decomposition, with results illustrated in Figures 11 and 12. No coking of the catalyst was observed, and up to 5 repeat experiments for the same length of time and at successive days yield the same H_2 production rates.

The average results of three repeat experiments are used in the figures below. The deviation between the repeat results and the averages were below 10%, accepted as fair in view of the lag time in the reactor-to-GC piping.

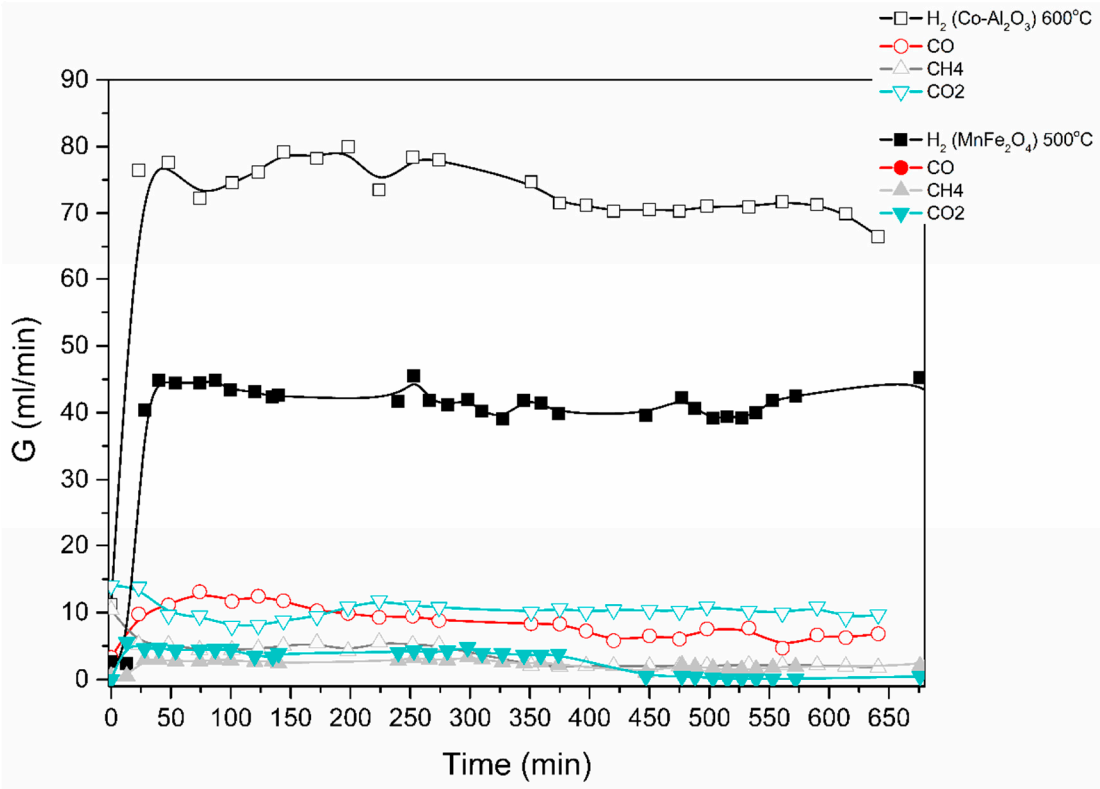

Figure 10. Catalytic decomposition of ethanol-water (1:6) mixture using Co-Al_2O_3 or $MnFe_2O_4$ catalyst. Results obtained in the electric furnace at the given temperatures.

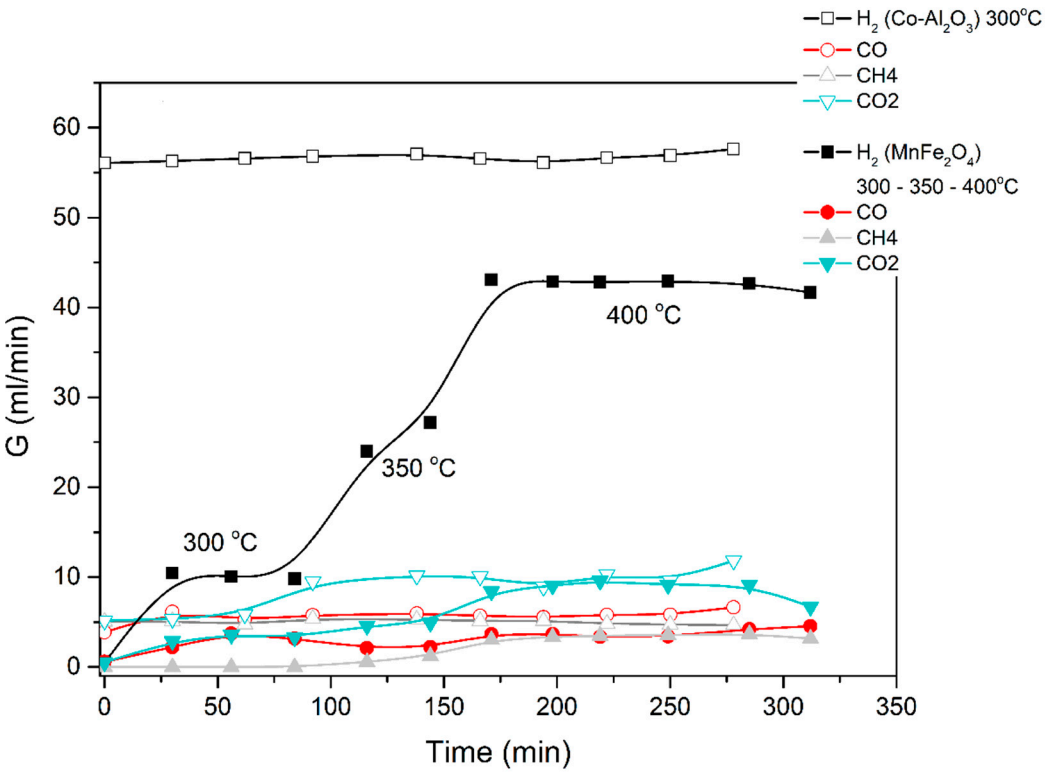

Figure 11. Catalytic decomposition of methanol-water (1:3) mixture using Co-Al_2O_3 or $MnFe_2O_4$ catalyst. Results obtained in the electric furnace at the given temperatures.

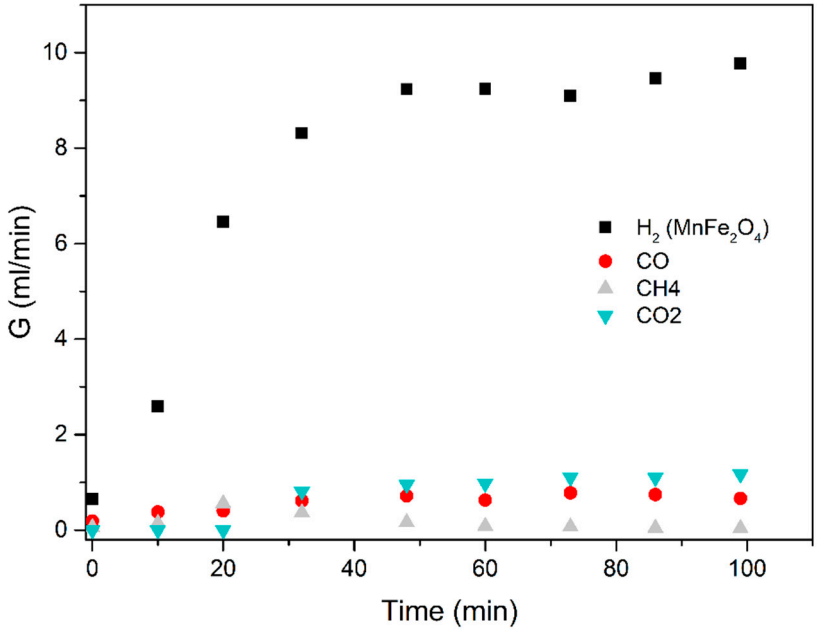

Figure 12. Methanol-water (1:3 mixture) using the $MnFe_2O_4$ catalyst. Results obtained in the electric furnace at 300 °C.

The results obtained demonstrate that excellent ethanol/methanol to H_2 conversions are achieved at low temperatures (300 to 500 °C is sufficient). In all the cases studied, the ratio of volumetric H_2 to CO_2 production was very high. Most of the feedstock carbon was detected as CO, CH_4 and acetone.

4.3. Tentative Techno-Economic Comparison of Different H_2 Production Technologies

From the experimental data and literature reports, the following comparison emerges (Table 5) for the levelized cost of hydrogen production (LCOH), for the GHG emission reduction potential and for the H_2 yield. Current production techniques of methane steam reforming, coal and biomass gasification and water electrolysis (using a renewable electricity source from wind turbines or photovoltaics) are compared with the novel methanol, methane and ethanol decomposition reactions.

Table 5. Techno-economic comparison (2017–2021).

	Methane Steam Reforming	Coal Gasification	Membrane Electrolysis (Renewable Energy)	Biomass Gasification	Methanol Steam Reforming	Ethanol Steam Reforming	Methane Decomposition
LCOH ($/kg H_2)	1.25	1.5	7.7	3 (for large scale) Otherwise > 5	1.8–2.2	1.5–2.0 (if acetone can be recovered and sold)	1.0–1.5 (if carbon black can be sold at 250–1000 $/ton)
GHG emission (kg CO_2-eq/kg H_2)	8.1–11	13–17	0	+/−0	>7	5–7	2.5
H_2 yield (%)	70–85	50–60	70	20–40	>90	60–80	75–80

From this summary table, it is clear that (i) biomass and coal gasification should be avoided because of the low H_2 yield and fairly high LCOH; (ii) all other systems have a fairly similar H_2 yield, although the GHG emission levels disfavor methane steam reforming and coal gasification; methane, methanol and ethanol decomposition reactions can reduce the CHG emission levels, while still achieving a competitive LCOH.

5. Conclusions

Since steel mills need to reduce their carbon footprint, the traditional high-temperature fossil-fuel-fired (>1200 °C) processes need to be avoided. The solution of the direct reduction of iron ore with hydrogen has high potential: (i) the process has a high conversion efficiency (up to 98%) at low temperatures (500–600 °C) and both the use of H_2 and the significantly lower operating temperatures reduce the energy consumption and fossil-based CO_2 emissions by over 75%; (ii) H_2 can be generated by competitive and environmentally friendly processes, as examined in the research.

The limitations of the present research must, however, be considered.

(i) Fe_2O_3 ore particles are of small size and cannot readily be processed by a H_2 stream in a fixed or fluidized bed. A novel vibrated fluidized bed was developed and shown capable of fluidizing µm-particles at very low superficial fluidization velocities. The small-scale experiments need to be confirmed on a pilot-scale. Vibrated fluidization of the fine Fe_2O_3 particles caused good fluidization and yielded a nearly constant pressure drop. An increase in external force due to vibration slightly increased the pressure drop. Despite an increase in the reaction temperature, vibration produces a nearly constant minimum fluidization velocity.

(ii) Although very interesting reduction reaction yields for fine Fe_2O_3 particles were obtained on a small-scale, it is important to investigate the production of such fine Fe_2O_3 feedstock on an industrial scale.

(iii) The remaining issue relates to the "green" production of H_2, currently based primarily on fossil fuel feedstock with a high degree of GHG emissions. Although steam reforming of ethanol and methanol offers an important potential, the methane process is preferred since its GHG emission potential is the most attractive (except for electrolysis and biomass gasification) while producing H_2 at a very interesting cost. Further pilot-scale experiments are required to confirm these initial lab-scale results.

(iv) To confirm the solar production potential, additional experiments will be conducted in the solar furnace as soon as the Direct Normal Irradiance values are higher (from July onwards).

Author Contributions: Conceptualization, J.B. and Y.D.; methodology, S.L., H.Z. and R.D.; validation, all authors; formal analysis, J.B., H.Z. and Y.D.; investigation, S.L., J.N. and Y.D.; resources, J.B.; data curation, all authors; writing—original draft preparation, J.B. and Y.D.; writing—review and editing, all authors; project administration, J.B.; funding acquisition, J.B. All authors have read and agreed to the published version of the manuscript.

Funding: This work was supported by the Beijing Advanced Innovation Centre for Soft Matter Science and Engineering of the Beijing University of Chemical Technology.

Institutional Review Board Statement: Not applicable.

Informed Consent Statement: Not applicable.

Data Availability Statement: The data that support the findings of this study are available on request to the corresponding author. The data are not publicly available until the Ph.D. of Yimin Deng has been released by KULeuven (expected 2022).

Conflicts of Interest: The authors declare no conflict of interest.

References

1. Wang, P.; Ryberg, M.; Yang, Y.; Feng, K.; Kara, S.; Hauschild, M.; Chen, W.-Q. Efficiency stagnation in global steel production urges joint supply- and demand-side mitigation efforts. *Nat. Commun.* **2021**, *12*, 2066. [CrossRef]
2. Sohn, H.Y.; Fan, D.-Q.; Abdelghany, A. Design of Novel Flash Ironmaking Reactors for Greatly Reduced Energy Consumption and CO2 Emissions. *Metals* **2021**, *11*, 332. [CrossRef]
3. Abolpour, B.; Afsahi, M.M.; Azizkarimi, M. Hydrogen reduction of magnetite concentrate particles. *Miner. Process. Extr. Metall.* **2021**, *130*, 59–72. [CrossRef]
4. Murakami, T.; Wakabayashi, H.; Maruoka, D.; Kasai, E. Effect of Hydrogen Concentration in Reducing Gas on the Changes in Mineral Phases during Reduction of Iron Ore Sinter. *ISIJ Int.* **2020**, *60*, 2678–2685. [CrossRef]

5. Patisson, F.; Mirgaux, O. Hydrogen Ironmaking: How It Works. *Metals* **2020**, *10*, 922. [CrossRef]
6. Zhang, A.; Monaghan, B.J.; Longbottom, R.J.; Nusheh, M.; Bumby, C.W. Reduction Kinetics of Oxidized New Zealand Ironsand Pellets in H2 at Temperatures up to 1443 K. *Metall. Mater. Trans. B* **2020**, *51*, 492–504. [CrossRef]
7. Bai, M.; Long, H.; Li, L.; Liu, D.; Ren, S.-B.; Zhao, C.-F.; Cheng, J. Kinetics of iron ore pellets reduced by H_2N_2 under non-isothermal condition. *Int. J. Hydrogen Energy* **2018**, *43*, 15586–15592. [CrossRef]
8. Wei, Z.; Zhang, J.; Qin, B.; Dong, Y.; Lu, Y.; Li, Y.; Hao, W.; Zhang, Y. Reduction kinetics of hematite ore fines with H_2 in a rotary drum reactor. *Powder Technol.* **2018**, *332*, 18–26. [CrossRef]
9. Bai, M.-H.; Long, H.; Ren, S.-B.; Liu, D.; Zhao, C.-F. Reduction Behavior and Kinetics of Iron Ore Pellets under H_2–N_2 Atmosphere. *ISIJ Int.* **2018**, *58*, 1034–1041. [CrossRef]
10. Lyu, Q.; Qie, Y.; Liu, X.; Lan, C.; Li, J.; Liu, S. Effect of hydrogen addition on reduction behavior of iron oxides in gas-injection blast furnace. *Thermochim. Acta* **2017**, *648*, 79–90. [CrossRef]
11. Elzohiery, M.; Sohn, H.Y.; Mohassab, Y. Kinetics of Hydrogen Reduction of Magnetite Concentrate Particles in Solid State Relevant to Flash Ironmaking. *Steel Res. Int.* **2017**, *88*, 1600133. [CrossRef]
12. Du, W.; Yang, S.; Pan, F.; Shangguan, J.; Lu, J.; Liu, S.; Fan, H. Hydrogen Reduction of Hematite Ore Fines to Magnetite Ore Fines at Low Temperatures. *J. Chem.* **2017**, *2017*, 1–11. [CrossRef]
13. Sohn, H.Y.; Mohassab, Y.; Elzohiery, M.; Fan, D.-Q.; Abdelghany, A. Status of the Development of Flash Ironmaking Technology. In *Applications of Process Engineering Principles in Materials Processing, Energy and Environmental Technologies*; The Minerals, Metals & Materials Series; Wang, S., Free, M., Alam, S., Zhang, M., Taylor, P., Eds.; Springer: Cham, Switzerland, 2017; pp. 15–23. [CrossRef]
14. Htet, T.T.; Yan, Z.; Spooner, S.; Degirmenci, V.; Meijer, K.; Li, Z. Gasification and physical-chemical characteristics of carbonaceous materials in relation to HIsarna ironmaking process. *Fuel* **2021**, *289*, 119890. [CrossRef]
15. Bhaskar, A.; Assadi, M.; Nikpey Somehsaraei, H. Decarbonization of the Iron and Steel Industry with Direct Reduction of Iron Ore with Green Hydrogen. *Energies* **2020**, *13*, 758. [CrossRef]
16. Vogl, V.; Åhman, M.; Nilsson, L.J. Assessment of hydrogen direct reduction for fossil-free steelmaking. *J. Clean. Prod.* **2018**, *203*, 736–745. [CrossRef]
17. He, K.; Zheng, Z.; Chen, H.; Hao, W. Reduction Behaviors of Hematite to Metallic Iron by Hydrogen at Low Temperatures. In *Energy Technology 2021: Carbon Dioxide Management and Other Technologies*; Springer: Cham, Switzerland, 2021; pp. 111–122.
18. Spreitzer, D.; Schenk, J. Fluidization behavior and reducibility of iron ore fines during hydrogen-induced fluidized bed reduction. *Particuology* **2020**, *52*, 36–46. [CrossRef]
19. Knop, K.; Kubiak, H. Process engineering and cost efficiency of steelmaking by means of hydrogen-based direct reduction. *Stahl und Eisen* **1996**, *116*, 55–64.
20. Hamadeh, H.; Mirgaux, O.; Patisson, F. Detailed Modeling of the Direct Reduction of Iron Ore in a Shaft Furnace. *Materials* **2018**, *11*, 1865. [CrossRef]
21. Ranzani da Costa, A.; Wagner, D.; Patisson, F. Modelling a new, low CO_2 emissions, hydrogen steelmaking process. *J. Clean. Prod.* **2013**, *46*, 27–35. [CrossRef]
22. Lazou, A.; van der Eijk, C.; Balomenos, E.; Kolbeinsen, L.; Safarian, J. On the Direct Reduction Phenomena of Bauxite Ore Using H2 Gas in a Fixed Bed Reactor. *J. Sustain. Metall.* **2020**, *6*, 227–238. [CrossRef]
23. Moldenhauer, P.; Linderholm, C.; Rydén, M.; Lyngfelt, A. Avoiding CO_2 capture effort and cost for negative CO_2 emissions using industrial waste in chemical-looping combustion/gasification of biomass. *Mitig. Adapt. Strateg. Glob. Chang.* **2020**, *25*, 1–24. [CrossRef]
24. Hoseinzadeh, S.; Stephan Heyns, P. Advanced Energy, Exergy, and Environmental (3E) Analyses and Optimization of a Coal-Fired 400 MW Thermal Power Plant. *J. Energy Resour. Technol.* **2021**, *143*, 082106. [CrossRef]
25. Tjahjono, T.; Ehyaei, M.A.; Ahmadi, A.; Hoseinzadeh, S.; Memon, S. Thermo-Economic Analysis on Integrated CO_2, Organic Rankine Cycles, and NaClO Plant Using Liquefied Natural Gas. *Energies* **2021**, *14*, 2849. [CrossRef]
26. Mahmoudan, A.; Samadof, P.; Hosseinzadeh, S.; Garcia, D.A. A multigeneration cascade system using ground-source energy with cold recovery: 3E analyses and multi-objective optimization. *Energy* **2021**, *233*, 121185. [CrossRef]
27. Torres, E.; Rodriguez-Ortiz, L.A.; Zalazar, D.; Echegaray, M.; Rodriguez, R.; Zhang, H.; Mazza, G. 4-E (environmental, economic, energetic and exergetic) analysis of slow pyrolysis of lignocellulosic waste. *Renew. Energy* **2020**, *162*, 296–307. [CrossRef]
28. Li, S.; Baeyens, J.; Dewil, R.; Appels, L.; Zhang, H.; Deng, Y. Advances in rigid porous high temperature filters. *Renew. Sustain. Energy Rev.* **2021**, *139*, 110713. [CrossRef]
29. Kong, W.; Tan, T.; Baeyens, J.; Flamant, G.; Zhang, H. Bubbling and Slugging of Geldart Group A Powders in Small Diameter Columns. *Ind. Eng. Chem. Res.* **2017**, *56*, 4136–4144. [CrossRef]
30. Fernandez, A.; Soria, J.; Rodriguez, R.; Baeyens, J.; Mazza, G. Macro-TGA steam-assisted gasification of lignocellulosic wastes. *J. Environ. Manag.* **2019**, *233*, 626–635. [CrossRef] [PubMed]
31. Geldart, D.; Baeyens, J. The design of distributors for gas-fluidized beds. *Powder Technol.* **1985**, *42*, 67–78. [CrossRef]
32. Haitao, W.; Sohn, H.Y. Reduction of Magnetite Concentrate Particles by H_2+CO at 1673 K. *ISIJ Int.* **2015**, *55*, 706–708.
33. Zhang, B.; Wang, Z.; Gong, X.; Guo, Z. Characterization of Precipitated Carbon by XPS and Its Prevention Mechanism of Sticking during Reduction of Fe_2O_3 Particles in the Fluidized Bed. *ISIJ Int.* **2013**, *53*, 411–418. [CrossRef]

34. Hsu, W.-Y.; Huang, A.-N.; Kuo, H.-P. Analysis of interparticle forces and particle-wall interactions by powder bed pressure drops at incipient fluidization. *Powder Technol.* **2018**, *325*, 64–68. [CrossRef]
35. Wank, J.R.; George, S.M.; Weimer, A.W. Vibro-fluidization of fine boron nitride powder at low pressure. *Powder Technol.* **2001**, *121*, 195–204. [CrossRef]
36. Al-Qodah, Z.; Al-Busoul, M.; Al-Hassan, M. Hydro-thermal behavior of magnetically stabilized fluidized beds. *Powder Technol.* **2001**, *115*, 58–67. [CrossRef]
37. Lucentini, I.; García Colli, G.; Luzi, C.D.; Serrano, I.; Martínez, O.M.; Llorca, J. Catalytic ammonia decomposition over Ni-Ru supported on CeO2 for hydrogen production: Effect of metal loading and kinetic analysis. *Appl. Catal. B Environ.* **2021**, *286*, 119896. [CrossRef]
38. Gu, Y.; Chen, X.; Zhao, S.; Zhang, Y. FeCe nanocomposite with high iron content as efficient catalyst for generation of CO_x-free hydrogen via ammonia decomposition. *J. Rare Earths* **2020**, *38*, 1053–1059. [CrossRef]
39. Lee, Y.-J.; Cha, J.; Kwak, Y.; Park, Y.; Jo, Y.S.; Jeong, H.; Sohn, H.; Yoon, C.W.; Kim, Y.; Kim, K.-B.; et al. Top-Down Syntheses of Nickel-Based Structured Catalysts for Hydrogen Production from Ammonia. *ACS Appl. Mater. Interfaces* **2021**, *13*, 597–607. [CrossRef] [PubMed]
40. Parker, L.A.; Carter, J.H.; Dummer, N.F.; Richards, N.; Morgan, D.J.; Golunski, S.E.; Hutchings, G.J. Ammonia Decomposition Enhancement by Cs-Promoted Fe/Al_2O_3 Catalysts. *Catal. Lett.* **2020**, *150*, 3369–3376. [CrossRef]
41. Ye, T.-N.; Lu, Y.; Kobayashi, Y.; Li, J.; Park, S.-W.; Sasase, M.; Kitano, M.; Hosono, H. Efficient Ammonia Synthesis over Phase-Separated Nickel-Based Intermetallic Catalysts. *J. Phys. Chem. C* **2020**, *124*, 28589–28595. [CrossRef]
42. Yu, Y.; Gan, Y.-M.; Huang, C.; Lu, Z.-H.; Wang, X.; Zhang, R.; Feng, G. Ni/La_2O_3 and $Ni/MgO–La_2O_3$ catalysts for the decomposition of NH_3 into hydrogen. *Int. J. Hydrogen Energy* **2020**, *45*, 16528–16539. [CrossRef]